Human Molecular Genetics, 2018, Vol. 27, No. 14 2454–2465

doi: 10.1093/hmg/ddy146
Advance Access Publication Date: 2 May 2018
Original Article

ORIGINAL ARTICLE

Functional variants in *TBX2* are associated with a syndromic cardiovascular and skeletal developmental disorder

Ning Liu[1,†], Kelly Schoch[2,†], Xi Luo[1,†], Loren D. M. Pena[2], Venkata Hemanjani Bhavana[1], Mary K. Kukolich[3], Sarah Stringer[3], Zöe Powis[4], Kelly Radtke[4], Cameron Mroske[4], Kristen L. Deak[5], Marie T. McDonald[2], Allyn McConkie-Rosell[2], M. Louise Markert[6], Peter G. Kranz[7], Nicholas Stong[8], Anna C. Need[9], David Bick[10], Michelle D. Amaral[10], Elizabeth A. Worthey[10], Shawn Levy[10], Undiagnosed Diseases Network (UDN)[11,‡], Michael F. Wangler[1,12,13], Hugo J. Bellen[1,12,13,14,15], Vandana Shashi[2,*] and Shinya Yamamoto[1,12,13,14,*]

[1]Department of Molecular and Human Genetics, Baylor College of Medicine, Houston, TX 77030, USA, [2]Division of Medical Genetics, Department of Pediatrics, Duke Health, Durham, NC 27710, USA, [3]Department of Genetics, Cook Children's Hospital, Fort Worth, TX 76102, USA, [4]Clinical Genomics, Ambry Genetics, Aliso Viejo, CA 92656, USA, [5]Department of Pathology, Duke University, Durham, NC 27710, USA, [6]Division of Allergy and Immunology, Department of Pediatrics, Duke Health, Durham, NC 27710, USA, [7]Division of Neuroradiology, Department of Radiology, Duke Health, Durham, NC 27710, USA, [8]Institute for Genomic Medicine, Columbia University, New York, NY 10032, USA, [9]Division of Brain Sciences, Department of Medicine, Imperial College London, London SW7 2AZ, UK, [10]HudsonAlpha Institute for Biotechnology, Huntsville, AL 35806, USA, [11]Undiagnosed Diseases Network, NIH Common Fund, Bethesda, MD 20892, USA, [12]Jan and Dan Duncan Neurological Research Institute, Texas Children's Hospital, Houston, TX 77030, USA, [13]Program in Developmental Biology and [14]Department of Neuroscience, Baylor College of Medicine, Houston, TX 77030, USA and [15]Howard Hughes Medical Institute, Houston, TX 77030, USA

*To whom correspondence should be addressed at: Department of Pediatrics, Box 103857 Duke University Medical Center, Durham, NC 27519, USA. Tel: +1 9196842036; Email: vandana.shashi@duke.edu (V.S.); Jan and Dan Duncan Neurological Research Institute, 1250 Moursund St, Houston, TX 77030, USA Tel: +1 8328248119; Email: yamamoto@bcm.edu (S.Y.)

Abstract

The 17 genes of the T-box family are transcriptional regulators that are involved in all stages of embryonic development, including craniofacial, brain, heart, skeleton and immune system. Malformation syndromes have been linked to many of the

[†]These authors contributed equally.
[‡]See Supplementary Material for full member list.
Received: March 7, 2018. **Revised:** April 7, 2018. **Accepted:** April 16, 2018

T-box genes. For example, haploinsufficiency of *TBX1* is responsible for many structural malformations in DiGeorge syndrome caused by a chromosome 22q11.2 deletion. We report four individuals with an overlapping spectrum of craniofacial dysmorphisms, cardiac anomalies, skeletal malformations, immune deficiency, endocrine abnormalities and developmental impairments, reminiscent of DiGeorge syndrome, who are heterozygotes for *TBX2* variants. The p.R20Q variant is shared by three affected family members in an autosomal dominant manner; the fourth unrelated individual has a *de novo* p.R305H mutation. Bioinformatics analyses indicate that these variants are rare and predict them to be damaging. *In vitro* transcriptional assays in cultured cells show that both variants result in reduced transcriptional repressor activity of TBX2. We also show that the variants result in reduced protein levels of TBX2. Heterologous over-expression studies in *Drosophila* demonstrate that both p.R20Q and p.R305H function as partial loss-of-function alleles. Hence, these and other data suggest that *TBX2* is a novel candidate gene for a new multisystem malformation disorder.

Introduction

Transcription factors of the T-box family play various roles throughout embryonic development (1) and have been reported to affect the development of numerous tissues including the face, skeleton, limb and heart (2,3). T-box family members, which share a conserved T-box domain that binds DNA in a sequence-specific manner, function as transcriptional repressors and/or activators (4,5). Mutations in 12 of the 17 human T-box genes have been associated with developmental syndromes that affect multiple organ systems including the heart and skeletal system (Supplementary Material, Table S1). For example, haploinsufficiency of *TBX1* (MIM: 602054) is responsible for many of the major manifestations of patients with DiGeorge syndrome (22q11.2 deletion syndrome, MIM: #188400) (6). These patients present with numerous and variable manifestations, including hypocalcemia related to parathyroid hypoplasia, thymic hypoplasia with immune deficiency, and outflow tract defects of the heart (7). Heterozygous mutations in the *TBX3* gene (MIM: 601621) cause autosomal dominant ulnar-mammary syndrome (MIM: #181450), a disease that is characterized by posterior limb deficiencies, apocrine/mammary gland hypoplasia, abnormal dentition, and genital anomalies (8). Heterozygous nonsense, frameshift and missense mutations in *TBX4* (MIM: 601719) have been identified as the cause of Ischiocoxopodopatellar syndrome, which exhibits characteristic skeletal abnormalities (9) (MIM: #147891). Haploinsufficiency of *TBX5* (MIM: 601620) causes Holt-Oram syndrome, which is characterized by cardiac and limb defects (10,11) (MIM: #142900). Variants in *TBX6*, *TBX15* and *TBX20* have also been associated with cardiac and/or skeletal anomalies.

The *TBX2* gene (MIM: 600747) has been implicated in heart (12), brain (13), eye (14), bone (15) and limb (16) development in mice. Copy number variations that include the *TBX2* gene have been associated with human skeletal and cardiac abnormalities, whereas a duplication of *TBX2* has been reported in a patient with skeletal malformations and cardiac defects (17). Further, a recurrent microdeletion at 17q23.1q23.2 encompassing *TBX2* and *TBX4* has been reported to co-segregate with human heart and limb defects (18). Although the aforementioned examples suggest that *TBX2* may be involved in human disease, an unequivocal relationship between *TBX2* pathogenic alterations and a Mendelian disorder has yet to be demonstrated.

Results

In this study, we identify four affected individuals in two unrelated families with heterozygous *TBX2* variants (Fig. 1A–F and Table 1). Common clinical manifestations include congenital cardiac defects, skeletal abnormalities, facial dysmorphia, variable developmental delay and endocrine system disorders (Fig. 1A–D, Table 1 and Supplementary Material, Fig. S1). Individuals 1–3 of family 1 were evaluated through the Undiagnosed Diseases Network (UDN) (19). Family 2 has one affected member (Individual 4). We utilized whole genome sequencing (WGS) and whole exome sequencing (WES) to identify the *TBX2* variants in families 1 and 2, respectively. The investigator groups for individuals 1–3 and 4 were connected through GeneMatcher (20), an online service that facilitates networking between researchers and clinicians interested in the same gene. Written informed consent was obtained from all individuals/guardians in accordance with institutional review board regulations.

Clinical presentation and family history of the four affected individuals

Individual 1 is a 7-year-old boy who manifests the following symptoms: congenital absence of the thymus and lack of functional T cells. He met the criteria for complete DiGeorge syndrome and was given an investigational allogeneic thymic transplant (Supplementary Material, Fig. S2). He also had unilateral cleft lip and palate; an atrial septal defect; camptodactyly of the third and fourth fingers; a unique cervical-vertebral fusion (Klippel-Feil anomaly); rib fusions; and scoliosis (Supplementary Material, Fig. S1). Individual 1 also developed autoimmune thyroiditis with hypothyroidism followed by hyperthyroidism. He currently has a normally functioning thyroid. Individual 1 had seizures in the neonatal period, but they have not recurred. Currently, cognition is in the average range, but academic achievement is below average. He displays attention-deficit hyperactivity disorder (ADHD) and autistic behaviors. Craniofacial features are remarkable for the presence of brachycephaly, widely spaced eyes, cupped ears and a short neck (Fig. 1A and Table 1).

Individual 2 (sister of individual 1) and individual 3, who is their mother, display similar but milder clinical presentations compared with individual 1. Individual 2's features include low T cell numbers meeting the criteria of partial DiGeorge syndrome; a cleft palate; a patent ductus arteriosus identified in infancy; short stature; Klippel-Feil anomaly; camptodactyly of the third and fourth fingers; hypertelorism; cupped ears and developmental delays (Fig. 1B, Table 1 and Supplementary Material, Figs S1 and S2). Individual 3 has low naïve T cells; a cleft palate; borderline low Parathyroid Hormone (PTH) with normal calcium levels; Klippel-Feil anomaly; and camptodactyly of the third and fourth fingers. She also has hypertelorism, cupped ears and normal cognition (Fig. 1C and Table 1). Incidentally, the father of Family 1 was reported to have a cleft lip, but no other overlapping features. Findings from immune evaluations on Patients 1–3 are documented in Supplementary Material, Supplementary Text.

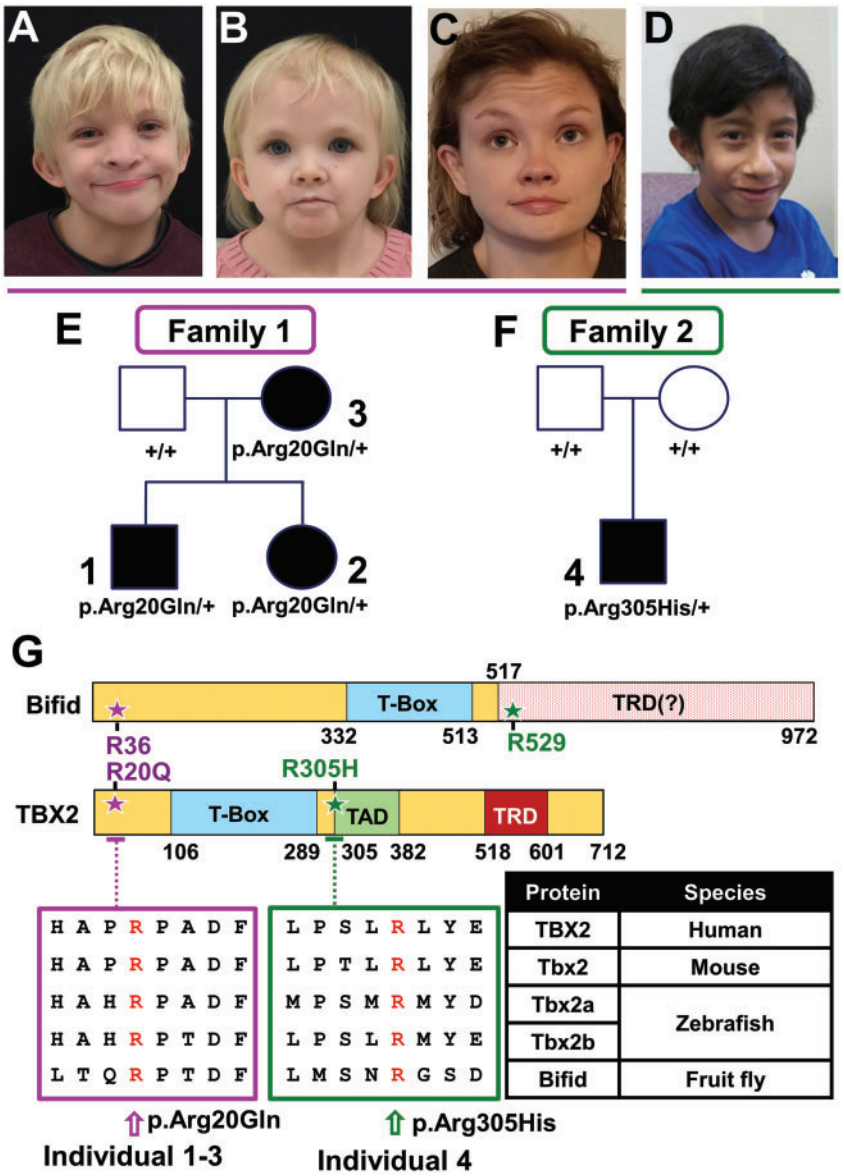

Figure 1. Clinical photographs and pedigree of four patients with *TBX2* variants that affect evolutionarily conserved amino acids. (**A**) Individual 1 at age 9 years; son of Individual 3. (**B**) Individual 2 at age 4 years; daughter of Individual 3. (**C**) Individual 3 at age 36 years; mother of Individuals 1 and 2. (**D**) Individual 4 at age 8 years. (**E**) Pedigree for Family 1 including Individuals 1–3. (**F**) Pedigree for Family 2 including Individual 4. (**G**) Top: Domain structure of *Drosophila* Bifid (Bi) and human TBX2 proteins. Variants identified in Patient 1–3 (p.R20Q) and 4 (p.R305H) and their corresponding amino acids in the fly protein are shown with a star. Bottom: Sequence alignments of the region surrounding the amino acids of interest in human, mouse, zebrafish and fruit fly. TRD, transcription repressor domain; TAD, transcription activation domain.

Individual 4 has short stature with growth hormone deficiency; a high arched and narrow palate; a double outlet right ventricle that was surgically corrected; congenital fusions of the thoracic spine and hemivertebrae with scoliosis; a triangular face; a depressed nasal bridge; cupped ears and developmental delays (Fig. 1D and Table 1).

Genomic analyses identified missense variants in *TBX2* gene

Chromosomal microarray results were normal for individuals 1 (EmArray Cyto6000-Oligonucleotide Array), 3 (Affymetrix Cytoscan HD) and 4 (Affymetrix Cytoscan HD), showing no evidence of chromosome 22q11.2 deletions or other pathogenic copy number changes. We performed WGS on individuals 1–3 along with the unaffected father (Supplementary Material, Table S2). We determined that individuals 1–3 in family 1 have a heterozygous variant c.59G > A (p.R20Q) in *TBX2*, and that individual 4 in family 2 harbors a *de novo* missense mutation, c.914G > A (p.R305H) in the same gene (Fig. 1E and F). We also demonstrated that individual 1 has a *de novo* likely pathogenic variant in *KCNQ2* (c.1057C > T, p.R353C), which explains the presence of neonatal seizures solely in him (Supplementary Material, Table S3).

To assess the likelihood of the pathogenicity of these variants, we examined *in silico* predictions regarding their impact on protein function, as well as population frequency (21). The following observations suggest that the *TBX2* variants we

Table 1. Clinical features of the patients with *TBX2* variants

	Individual 1 (son)	Individual 2 (daughter)	Individual 3 (mother)	Individual 4
Family		Family 1		Family 2
Variant		c.59G>A/p.R20Q		c.914G>A/p.R305H
		Heterozygous		Heterozygous
Inheritance		Autosomal dominant		*de novo*
Bioinformatic signature		Polyphen: 0.885		Polyphen: 0.973
		CADD: 24		CADD: 35
		gnomAD: 2/89, 521		gnomAD: 0/89, 521
Age	9 years	6 years	36 years	8 years
Gender	Male (son).	Female (daughter).	Female (mother).	Male
Race/ethnicity	Causacian/Non-hispanic.	Causacian/Non-hispanic.	Causacian/Non-hispanic.	Caucasian/Hispanic.
growth parameters	Height 36th percentile. Head circumference 52nd percentile.	Height 3rd percentile. Head circumference 24th percentile.	Height 18th percentile. Head circumference 75th percentile.	Height 2nd percentile. Head circumference 4th percentile.
Developmental delay/ intellectual disability	Autistic behaviors and ADHD. Average intelligence.	Mild delays in development.	Normal intelligence.	Mild cognitive and academic impairments.
Dysmorphic features	Triangular face, hypertelorism with epicanthal folds, depressed nasal bridge, cupped right ear, low set ears.	Hypertelorism with epicanthal folds, glabellar hemangioma, low set ears with over folded helices.	Hypertelorism with epicanthal folds, cupped ears, webbed neck.	Triangular face, depressed and broad nasal tip, cupped and low set ears, low anterior hairline.
Orofacial clefting	Cleft palate and unilateral cleft lip.	Cleft palate.	Cleft palate.	High arched, narrow palate.
Cardiac	Atrial septal defect, closed.	Patent ductus arteriosus, closed.	None.	Double outlet right ventricle, valvular pulmonic stenosis.
Immune	Absent thymus, 'complete' DiGeorge. Required thymic transplant.	Abnormal T and B cells, 'partial' DiGeorge.	Very low naïve T-cells: CD4 and CD8.	No symptoms, no formal immune function tests.
Skeletal	Camptodactyly of 3rd and 4th fingers, Klippel Feil (fusion of C2–C4) and Sprengel deformities, fusion of 4th–5th ribs, scoliosis of thoracic spine.	Camptodactyly of 3rd and 4th fingers Klippel Feil and Sprengel deformities on clinical examination.	Camptodactyly of 3rd and 4th fingers, Klippel Feil (fusion of C3–C4) and Sprengel deformities.	Congenital fusions of the thoracic spine-T5, and T12-L2 with open laminae posteriorly, hemivertebrae between T10 and T11, scoliosis and kyphosis.
Endocrine	Hashimoto's thyroiditis.	Hypoparathyroidism.	Borderline low PTH.	Growth hormone deficiency, normal thyroid studies.
Other	Benign neonatal seizures due to *de novo* likely pathogenic variant in *KCNQ2*, correctopia of pupils of the eyes.	No recent eye examination.	Medullary nephrocalcinosis of the kidneys, correctopia of pupils of the eyes.	Inguinal hernia, chordee, undescended testicle.

identified are detrimental to protein function. First, the p.R20Q and the p.R305H variants are predicted to be deleterious by SIFT (22), PolyPhen-2 (23), MutationTaster2 (24) and CADD models (25) (Table 1). Second, *TBX2* has a high probability of loss-of-function intolerance (pLI = 0.96), with only one loss-of-function variant observed despite 14.5 expected in 60, 706 individuals in the ExAC (Exome Aggregation Consortium) database (26). Third, with a constraint score of 3.37 (6.9th percentile), *TBX2* is highly intolerant of missense variants (172 observed versus 290 expected in ExAC) (26). Fourth, the probability of *TBX2* being associated with an autosomal dominant condition is very high, as evidenced by a score of 0.999 on the basis of DOMINO (27).

We next sought to determine whether the variants we detected are found in control populations by searching internal and public databases. The p.R20Q variant was observed in 1/2,865 internal controls from a hemophilia cohort from Columbia University, which is where the WGS data analyses for family 1 were performed. The variant found in this control sample had good quality metrics, with no evidence of mosaicism (50% alt allele reads). The p.R20Q variant was also observed in 2/89, 521 individuals in the gnomAD (genome Aggregation Database), but the variant entries did not pass a basic quality filter, likely as a result of low coverage. Finally, the p.R305H variant was not present in the Columbia control cohort, the ExAC or gnomAD databases (26). This information strongly suggests that p.R305H is likely to have functional consequences. The p.R20Q variant is also a good candidate for causation considering that both variants affect highly conserved residues

across vertebrate and invertebrate species (Fig. 1G). Thus, we deemed functional evaluation of these variants to be valuable, especially given the variability of the phenotypes observed within the same family.

To examine if *TBX2* copy number gain or loss of is associated with phenotypes similar to those described in our patients, we searched the DECIPHER database (28) and found 13 chromosomal deletions and six duplications encompassing *TBX2*. The deletions vary in size from ~190 kb to 66 Mb, whereas the duplications vary in size from ~130 kb to ~19 Mb. The phenotypes listed for these individuals include intellectual impairments and congenital heart disease; however, the specific contribution of *TBX2* to these phenotypes is difficult to infer. Finally, a recurrent microdeletion at 17q23.1q23.2 that includes *TBX2* has been associated with heart defects and limb abnormalities (18). Hence, copy number variation of *TBX2* has been associated with disease phenotypes that are consistent with the symptoms observed in the families presented here.

Disease associated variants diminish the transcriptional repressor function of TBX2 in HEK293T cells by affecting protein production or stability

To assess the consequences of the two variants on the transcription repressor activity of TBX2 (29,30), we performed a luciferase activity assay driven by two different promoters with T-box transcription factor binding sites in HEK293T cells (31). The full-length reference (wild-type) or variant *TBX2* cDNAs were expressed from a mammalian cell expression vector (pcDNA-DEST40) together with a firefly luciferase reporter vector (2xTtkGL2) containing two copies of the palindromic T-box sites at a promoter-proximal position (Fig. 2A). The transfection efficiency was controlled by normalizing the signals against the co-transfected β-Galactosidase (β-GAL) activity. As expected, the reference TBX2 repressed the promoter activity by approximately five-fold (an 80% reduction) (Fig. 2B). In contrast, the p.R20Q and p.R305H variants exhibited an approximately 30% and 35% reduction, respectively, suggesting that the two variants behave as hypomorphic variants (Fig. 2B). The same results were also obtained through an independent assay using nano-Luciferase as a reporter with a minimal promoter (Supplementary Material, Fig. S3A and B).

To assess the molecular mechanism by which the loss of repression activity occurs, we first analyzed TBX2 expression in protein extracts from HEK293T cells transfected with reference or variant *TBX2* cDNA. The extracts were probed with an antibody raised against the middle region of human TBX2 protein (amino acids 98 to 338). Interestingly, we detected approximately 20% of the TBX2 protein with the p.R20Q variant and about 30% of the p.R305H variant when compared with the reference protein (Fig. 2C–F). This reduction of TBX2 protein observed in p.R20Q and p.R305H variants suggest that these amino acid changes affect protein production or stability.

We next examined the nuclear localization of the transiently transfected TBX2 proteins in HEK293T cells. The reference TBX2, as well as both variant proteins were found to be enriched in the nucleus, suggesting that these amino acid changes do not alter the nuclear localization of TBX2 (Supplementary Material, Fig. S3C). In summary, the reporter-based cell assays reveal that the p.R20Q and p.R305H variants have reduced transcription repression activity that is likely owing to the reduced protein levels because neither of the variants affect nuclear localization of TBX2.

Ectopic expression of wild-type fly bifid and reference human TBX2 causes a strong developmental and functional defect in the eye, and these effects are significantly diminished by patient variants

To further investigate the functional significance of the observed variants affecting the *TBX2* gene *in vivo*, we first attempted to use a recently established 'humanization' strategy to annotate disease associated variant functionality in *Drosophila* (32–34). *TBX2* belongs to the TBX2 subfamily of T-box transcription factors, which also includes *TBX3*, *TBX4* and *TBX5* (Supplementary Material, Fig. S3A). These four T-box genes have a single common *Drosophila melanogaster* ortholog *bifid*, also known as *optomotor blind (omb)*. Loss of *bifid* causes lethality as well as developmental defects in flies (35,36). Unfortunately, we were unable to rescue a *Drosophila bifid* loss-of-function mutant using the human reference or variant TBX2 proteins (Supplementary Material, Supplementary Text and Fig. S5A–C). Moreover, this clean fly mutant allele was not rescuable with a fly Bifid protein using the T2A-Gal4 system (Supplementary Material, Fig. S5C), likely owing to *bifid* being highly sensitive to dosage (37,38). Hence, we resorted to the following tissue specific overexpression assays to assess the effect of the variants *in vivo*.

To evaluate the functional significance of the p.R20Q and p.R305H variants in *TBX2 in vivo*, we performed heterologous over-expression studies using tissue specific Gal4 drivers (39). We first confirmed that fly Bifid and human TBX2 (both reference and variants) localize to the nucleus (Supplementary Material, Fig. S6), similar to our observation in HEK293T cells (Supplementary Material, Fig. S3C). Next, we drove the expression of these proteins using an *eyeless(ey)-Gal4* driver in the developing fly visual system, which consists of the eye imaginal discs and parts of the brain (40). Ectopic expression of wild-type (WT) *bifid*, reference TBX2 and the two variant TBX2 proteins caused a significantly different degree of toxicity, as quantified by lethality and fly eye size. *ey-Gal4* driven reference human TBX2 caused lethality in a large fraction of animals and a greater reduction in eye size than the fly Bifid did (Fig. 3A and B). Strikingly, both p.R20Q and p.R305H human TBX2 variant proteins were much less potent than the reference protein, indicating that they function as partial loss of function alleles (Fig. 3A and B). This finding is consistent with our cultured cell based studies (Fig. 2).

To further explore the functional consequences of expression of the above proteins in mature versus developing visual system, we expressed the UAS-*bifid* and UAS-*TBX2* constructs in the adult photoreceptors using the *Rhodopsin1*(*Rh1*)-*Gal4* driver. The cDNAs expressed under the control of this driver do not affect the development of the eye because the expression of the cDNA is initiated in late pupal development, just prior to eclosion (41). We measured photoreceptor activity in adult flies using electroretinograms (ERG) (42). ERG recordings reveal two key features: the 'on' and 'off' transients (green and blue dotted circles in Fig. 3C) that reflect synaptic transmission between pre-synaptic photoreceptors and post-synaptic neurons, and the amplitude of the photoreceptor depolarization (red bracket in Fig. 3C) which is a measure of the phototransduction activity. Expression of WT Bifid and TBX2 driven by *Rh1-Gal4* caused a severe loss of synaptic transmission phenotype as evidenced by loss of the 'on' and 'off' transients (Fig. 3C–E) and severe defects in phototransduction as measured by the decreased amplitude (Fig. 3C and F). In addition, an abnormal PDA (prolonged

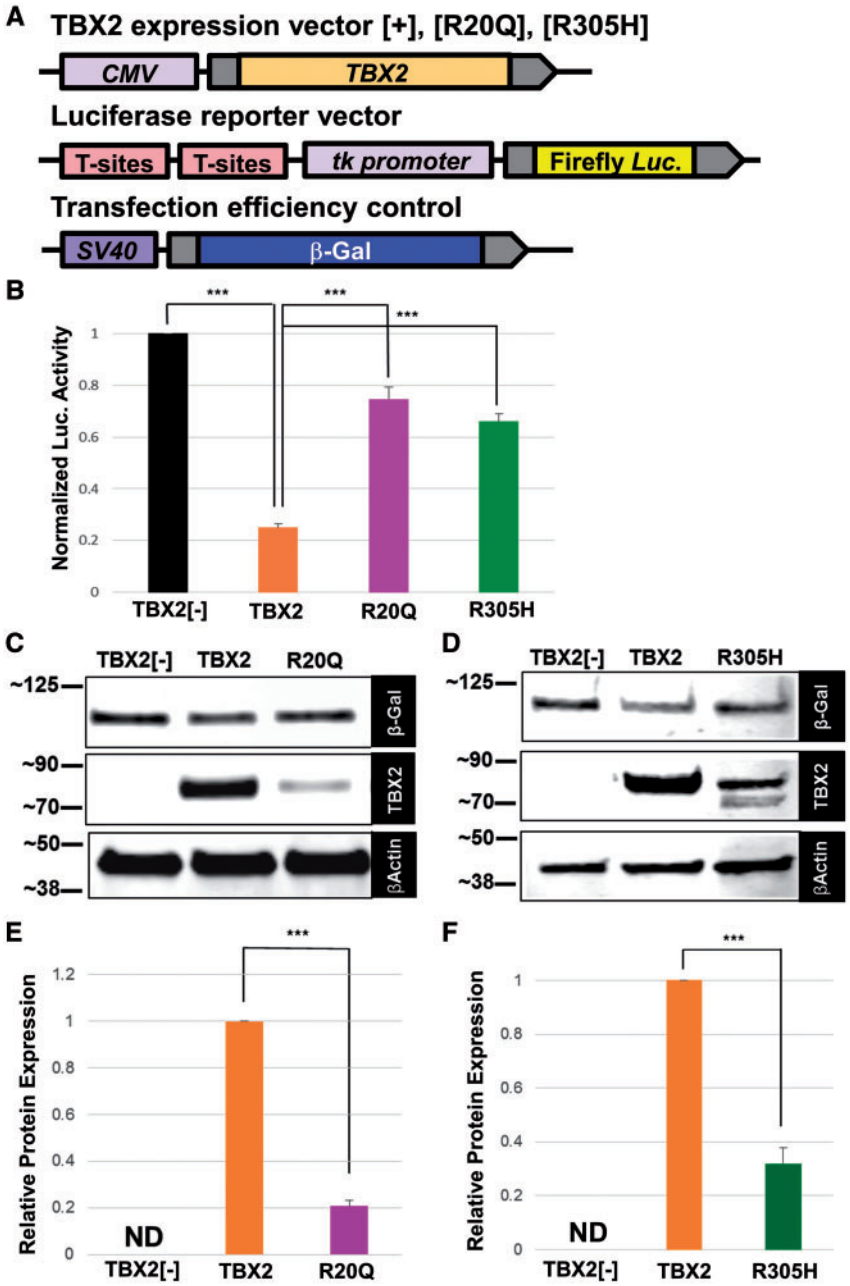

Figure 2. Disease-associated variants diminish the transcriptional repressor function of TBX2 in HEK293T cells through affecting protein production or causing protein instability. (**A**) Schematic illustration of vectors used for the reporter assays in cultured cells. Expression vectors (pcDNA-DEST40) driving a full-length reference (wild-type) or variant *TBX2* cDNA by a CMV promoter were transiently transfected into HEK293T cells together with a firefly luciferase reporter vector (2xTtkGL2) containing two copies of the palindromic T binding sites at a proximal position relative to the herpes simplex thymidine kinase (tk) promoter. Luciferase activities were measured and normalized against β-Galactosidase expressed under the simian virus 40 (SV40) promoter from a transfection efficiency control vector (pSV-β-Gal) that was co-transfected. (**B**) TBX2 represses the expression of fire fly Lluciferase approximately 4- to 5-fold (orange) relative to empty expression vector control (black). TBX2[R20Q] and TBX2[R305H] show poor transcription repressor activity (purple and green), indicating severe loss of repressor function. Reporter assays were carried out by repeating the triplet transfection at least four times ($n = 12$) under independent experimental conditions. The endogenous luciferase activity was defined as 100%. Results are represented as mean ± SEM. *$P < 0.05$, ***$P < 0.001$. (**C**) Comparison of reference and variant TBX2 protein levels upon transient-transfection into HEK293T cells. Protein expression was examined by western blot of cell extracts. Protein load was normalized against β-actin, and transfection efficiency was controlled by β-GAL. TBX2[R20Q] expression level was significantly decreased compared the reference TBX2, suggesting that protein production or stability is significantly reduced. (**D**) TBX2[R305H] expression level was also significantly decreased compared the reference TBX2, suggesting that protein production or stability is significantly reduced. (**E**) Quantification of TBX2 levels on the basis of western blots. Expression level of TBX2[R20Q] is approximately 4- to 5-fold less than wild-type TBX2. Results are represented as mean ± SEM. ***$P < 0.001$. (**F**) Quantification of TBX2 levels on the basis of western blots. Expression level of TBX2[R305H] is approximately 3- to 4-fold less than wild-type TBX2. Results are represented as mean ± SEM. ***$P < 0.001$. ND: not detected.

A

ey-Gal4>	UAS-bifid	UAS-TBX2	UAS-TBX2 R20Q	UAS-TBX2 R305H
Percent Eclosed Flies	44.5%	15.2%	40.5%	76.8%
Percent Severe reduction in eyes size	63%	71.4%	16.7%	5.4%

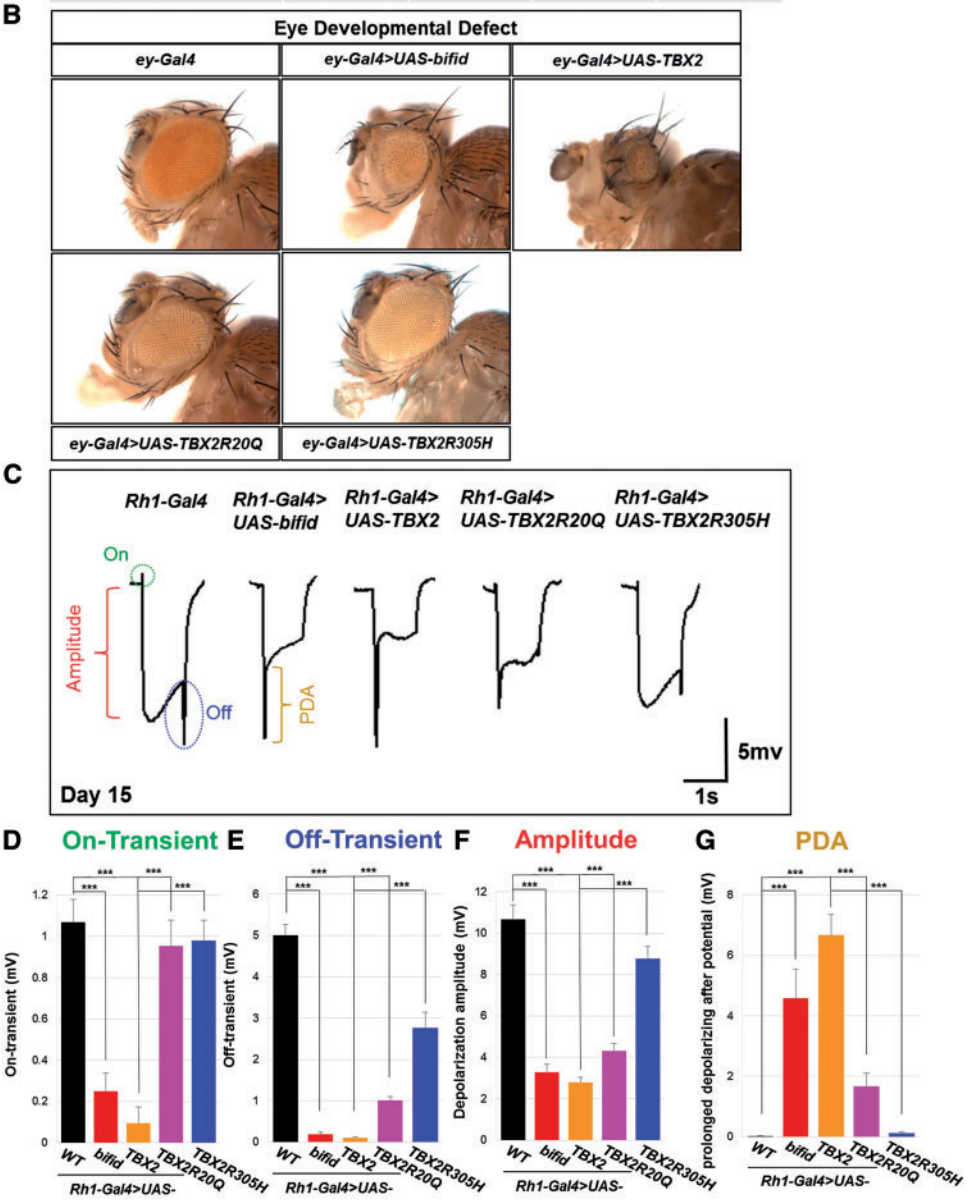

Figure 3. Over-expression of wild-type Bifid or reference human TBX2 causes a strong developmental and functional defect in the eye, and these effects are milder in *TBX2* that carry patient variants. (**A, B**) The *ey-Gal4* driver was used to drive expression of fly *bifid* and human *TBX2* cDNAs in the developing fly visual system (eye imaginal discs and parts of the brain). (A) Expression of ectopic *bifid*, *TBX2* and variants exhibit pupae lethality to some degree. Disease-associated TBX2 variant proteins are less toxic than reference protein, indicating that they function as partial loss-of-function alleles in this context. (B) Images of adult heads of *ey-Gal4* (control); *ey-Gal4>UAS-bifid*, *ey-Gal4>UAS-TBX2[+]*, *ey-Gal4>UAS-TBX2[R20Q] and ey-Gal4>UAS-TBX2[R305H]*. Expression of wild-type *bifid* and reference *TBX2* results in a greater reduction in eye size than expression of the variants, indicating *TBX2* mutant variants behave as partial loss-of-function mutations in this context as well. (**C–G**) Ectopic expression of fly *bifid* and human *TBX2* transgenes expressed in the photoreceptors by *Rh1-Gal4* cause more severe ERG (electroretinogram) defects compared with TBX2[R20Q] and TBX2[R305H]. Expression of *bifid* and *TBX2* driven by *Rh1-Gal4* exhibits a loss of the on-transients (D) and off-transients (E), indicators of synaptic communication between the pre-synaptic photoreceptors and post-synaptic lamina neurons. Similarly, over-expression of these genes dramatically decreased the amplitude of depolarization, a measure of phototransduction, and exhibited an abnormal PDA (prolonged depolarization after potential) phenotype. TBX2[R20Q] and TBX2[R305H] show much less severe defect, again suggesting that this allele behaves as a hypomorphic allele.

depolarization after potential) phenotype was observed in these flies, which was previously reported with blue light induction (Fig. 3C and G) (43). Both the *TBX2* p.R20Q and p.R305H variants caused much less severe ERG defects compared with the reference cDNA, illustrating that these variants behave as hypomorphic alleles not only during development, but also in fully developed neurons (Fig. 3C–G). Taken together, these heterologous over-expression studies in *Drosophila* provide support for the hypothesis that p.R20Q and p.R305H function as partial loss-of-function alleles.

Discussion

Herein, we present clinical, genomic, bioinformatic and functional evidence supported by prior experimental data in model organisms that supports the hypothesis that *TBX2* is a strong candidate for the phenotypes of four individuals affected by a multisystem malformation disorder. *Drosophila bifid* has been reported to regulate optic lobe (35) and wing (36) development by controlling cell proliferation, viability and cell migration. In zebrafish, loss-of-function mutants of the duplicated *TBX2* co-orthologs *tbx2a* and *tbx2b* show conspicuous phenotypes including abnormal heart contraction, heart edema, atrioventricular canal formation and heart looping defects; abnormal epithalamus, parapineal, and dorsal habenular nucleus development; increased rod and decreased cone photoreceptor numbers; and otic vesicle defects (44,45). Homozygous *Tbx2* knockout mice exhibit atrioventricular canal defects, pericardial edema, cleft palate, polydactyly, and embryonic lethality, which indicates the crucial role for *Tbx2* during development, and in particular cardiac development (12,46). The phenotypes reported in these prior studies provide additional support for the notion that the cardiac, palate and skeletal defects observed in our patients are caused by variants in the *TBX2* gene.

Phenotypic studies in the hearts of $Tbx1^{-/-}$; $Tbx2^{-/-}$ and $Tbx1^{-/-}$; $Tbx3^{-/-}$ double mutant mouse embryos indicate that *Tbx1* is required for the expression of *Tbx2* and *Tbx3* in neural crest (NC)-derived mesenchyme and pharyngeal endoderm (47). *Tbx1*, *Tbx2* and *Tbx3* potentially comprise a T-box regulatory network that controls pro-proliferative fibroblast growth factor and Sonic hedgehog signaling, as well as pro-differentiation bone morphogenetic protein (BMP) signaling during pharyngeal and outflow tract development. The patients with *TBX1*-haploinsufficient 22q11.2 deletion (DiGeorge) syndrome display variable severity of cardiovascular malformations, which overlaps the symptoms of our patients carrying *TBX2* variants (48). The syndromic orofacial clefting observed in our patients is also a common phenotype associated with the *TBX1* and *BMP4* (MIM: 112262, #600625) genes. Prior studies on *Tbx1*–*Tbx2* interaction during heart development in mice, and the overlapping phenotypes observed in the two syndromes further support our hypothesis that *TBX2* variants are the genetic cause of the clinical manifestations in our patients. Moreover, these manifestations are consistent with aberrant development of structures derived from the pharyngeal apparatus.

Because the p.R20Q and p.R305H variants decrease protein levels of TBX2 and behave as hypomorphic alleles when tested in cultured cells and *in vivo* in *Drosophila*, we postulate a loss-of-function mechanism. Phenotype expression is often variable for developmental disorders, as observed in the case for the *TBX2* gene described here (Table 1). The affected sister and mother (individuals 2 and 3, respectively) in family 1 display similar phenotypes but have clearly milder presentations than individual 1. However, individual 4, who is unrelated to individuals 1–3, displays remarkably similar facial features, and skeletal and cardiac defects (Fig. 1A–D and Table 1). Considering that both the *Drosophila bifid* and human *TBX2* genes are sensitive to dose-dependent effects (37,38), individuals with subtle differences in TBX2 protein expression levels that may vary across different tissues, could present variable phenotypes. This notion is supported by the fact that the T-box genes are differentially expressed at multiple stages of embryonic development across different tissues (49).

The phenomenon of the p.R20Q variant being seen in at least one control individual is observed in other known disease-associated genes, such as those of the *ASXL* gene family, and the *ARID1B* gene, wherein rare pathogenic variants are occasionally observed in presumably healthy controls (50–52). Possible explanations for this phenomenon include variable expressivity and reduced penetrance; indeed, a recent report has confirmed that incomplete penetrance of Mendelian disease is more common than realized (53,54). Although these two heterozygous variants remain the strongest candidates for disease in our two unrelated families, additional similarly affected individuals with *TBX2* variants are required to conclusively show that the specific human phenotypes described herein are due to *TBX2* alleles (55). Nevertheless, our data provide strong support for *TBX2* as an additional T-box gene linked to a developmental disease (Supplementary Material, Table S1). Importantly, our functional assays and data they generate provide a means to test whether novel *TBX2* variants are deleterious to the function of this essential developmental gene.

Materials and Methods

Human subjects and recruitment

Consent for publication was obtained from all subjects or the subjects' parents, and procedures were followed in accordance with guidelines specified by Institutional Review Boards and Ethics Committees of each institution. Individual 1 was enrolled in IRB Protocol Pro00013734 'Thymus Transplantation with Immunosuppression, #884,' NCT00579709. This protocol was conducted under Investigational New Drug (IND) Application #9836 with the Food and Drug Administration. Individuals 2 and 3 were enrolled in IRB Protocol Pro000133328 'Evaluation of Immune Function in Inherited Immunodeficiency #603.'

DNA sequencing methods

Following DNA extraction from each member of the quad, the genome was captured using the QIAsymphony DSP DNA Midi Kit (96) version 1 (Qiagen) and sequenced using Illumina HiSeq X. Variants were analyzed using the CarpeNovo software (56). Individual 4 underwent trio WES on a clinical basis through a commercial laboratory (57,58) (Supplementary Material, Table S2) and following DNA extraction from the trio, the exome was captured using SeqCap EZ VCRome 2.0 (Roche NimbleGen) and sequenced using Illumina HiSeq2500.

Cloning and mutagenesis

TBX2 human cDNA (Invitrogen Ultimate ORF clone: IOH29393, GenBank: BC052566.1) was a kind gift from Dr. Kenneth L. Scott at Baylor College of Medicine. This clone is in a pDONR 221 backbone vector and Gateway LR cloning method was used to shuttle the cDNA into the destination vectors (pcDNA-DEST40 vector for mammalian cell expression and pUASg-HA.attB

vector for *Drosophila* transgenesis). Because the original cDNA clone contained a translational stop codon after the coding sequence (closed clone), C'-tags that are present in the expression plasmids (V5–6xHis for pcDNA-DEST40, 3xHA for pUASg-HA.attB) are not fused to the translated protein. The reagents for Gateway cloning were purchased from Invitrogen of the Thermo Fisher Scientific corporation (Catalog number: 12535–029). The point mutations of *TBX2* in the human cDNA were engineered using the Q5 Site-Directed Mutagenesis Kit from NEB (Catalog number: E0554S). To generate a nano-Luciferase based T-box reporter construct (2TpNL3.1), we commercially synthesized two complementary single stranded oligonucleotides that contain two palindromic T-box binding site sequences (underlined in the following) joined together with a 10 bp linker sequence and flanked by restriction enzyme site (EcoRV and XhoI) sequences.

2T(*Xho*I-*Eco*RV)Forward: TCGAGAATTTCACACCTAGGTGTGAAATTCGTCGCCGCAAATTTCACACCTAGGTGTGAAATTGAT

2T(*Xho*I-*Eco*RV)Reverse: ATCAATTTCACACCTAGGTGTGAAATTTGCGGCGACGAATTTCACACCTAGGTGTGAAATTC

After annealing the two oligos, the T-box binding sites were cloned into pNL3.1 (Promega) digested by *Eco*RV and *Xho*I. Firefly luciferase based reporter construct (2xTtkGL2) and transfection efficiency control vector (pSV-β-Gal) were gifts from Dr. Antonio Baldini (59,60).

Mammalian cell culture and luciferase-based transcription reporter assays

HEK293T cells were plated in 12-well dishes at 20–30% confluence in Dulbecco's Modified Eagle's Medium (Life Technologies) supplemented with 1% sodium pyruvate, 1% L-glutamine, 10% FBS and antibiotics (penicillin-streptomycin) at 37°C and 5% carbon dioxide. After overnight culture, cells were transfected by Lipofectamine 2000 (Life Technologies) with 200 ng of TBX2-expressing constructs [TBX2(reference or variant)-pcDNA-DEST40], 400 ng of reporter plasmids (2xTtkGL2 or 2TpNL3.1) and 50 ng of LacZ-expressing plasmid (pSV-β-Gal). Cells were harvested 48 h later and washed once with phosphate-buffered saline (PBS). For luciferase assays, cells from each well were lysed with 250 µl of 1× Passive Lysis Buffer (Promega: E1941) by shaking for 15 min at room temperature (RT). Luciferase activity was measured from 80 µl of cell lysate with a luminometer (FLUOstar OPTIMA, BMG Labtech). The internal control β-galactosidase activities were obtained from 40 µl of the cell lysate. Each assay was performed in technical duplicates and repeated at least three times. Proteins from the cell extracts were separated by running on a 4–20% gradient gel (Mini-PROTEAN TGX™ Precast Protein Gels, Bio-Rad), and proteins were detected using the Odyssey system (Li-COR). Protein loading was normalized against β-Actin, and transfection efficiency was controlled by β-galactosidase. The primary anti-TBX2 antibody (rabbit, used 1:500) was purchased from Thermo Fisher Scientific (Catalog #: PA5–29768), and secondary antibody (anti-rabbit IgG IRDye 800CW) was purchased from Li-COR. The band intensity was quantified by ImageJ (https://imagej.nih.gov/ij/; date last accessed April 6, 2018).

Immunostaining, fluorescence imaging and confocal microscopy

For immunostaining of cultured human cell lines, HEK293T cells transfected with expression constructs for reference and variant cDNAs (see luciferase assay section for the transfection protocol) were fixed with 4% formaldehyde/1× PBS for 10 min at RT, washed twice with 1× PBS, and incubated in 0.25% saponin/PBS/FBS for 4 h at RT. Fixed cells were incubated with anti-TBX2 primary antibody (used 1:500, Thermo Fisher Scientific) at 4°C overnight. After washing with 1× PBS three times (5 min/each), cells were incubated with anti-rabbit fluorescent secondary antibody (Alexa Fluor 488 conjugated, 1:500, Jackson ImmunoResearch) together with fluorescent phalloidin (Alexa Fluor 680 conjugated, Thermo Fisher Scientific) for 1 h at RT. Cells were mounted in DAPI Fluoromount-G (SouthernBiotech) and imaged with a LSM880 confocal microscope (Zeiss) under a 63× oil immersion objective lens, and images were analyzed using the Zen software (Carl Zeiss).

For immunostaining of larval brains and wing imaginal discs from *Drosophila*, third instar larvae were dissected for in 1× PBS and fixed in 4% formaldehyde for 30 min at RT and washed in PBS with 0.2% Triton X-100. The samples were then blocked by incubating them for 1 h at RT in 10% NGS (normal goat serum)/PBS/0.2% Triton X-100 and stained with primary antibodies diluted in 10% NGS/PBS/0.2% Triton X-100 overnight at 4°C. Anti-TBX2 (rabbit, 1:200, Thermo Fisher Scientific) and anti-Bifid (rabbit, 1:200, a gift from Dr. Gert Pflugfelder) (38) antibodies were used as primary antibodies. The samples were washed and incubated with secondary antibodies (with or without DAPI) for 1 h at RT. For examination of GFP, signal was enhanced by staining the tissues with an anti-GFP antibody conjugated to FITC (Abcam). Samples were mounted in Vectashield (Vector Labs, Burlingame, CA), imaged with a LSM880 confocal microscope (Zeiss) and processed using Photoshop (Adobe).

Whole-mount immunolabeling of the adult brain was performed as previously described (61). Briefly, brains were dissected in 1× PBS and fixed overnight in 4% paraformaldehyde in PBS on ice, transferred to 4% paraformaldehyde in PBS with 2% Triton X-100 at RT and vacuumed for 1 h to remove the air sacs and left overnight in PBS with 2% Triton X-100 at 4°C. GFP signal was enhanced by staining the brains with an anti-GFP antibody conjugated to FITC (Abcam). Finally, brains were cleared and mounted in RapiClear (SunJin Lab Co., Taiwan) and imaged with a LSM880 confocal microscope (Zeiss) under a 20× C-Apochromat water immersion objective lens. Images and processed using Photoshop (Adobe).

Drosophila genetics

bi[T2A-Gal4] line was generated from a MiMIC line *Mi{MIC}bi*^{MI08152} via Recombinase-Mediated Cassette Exchange (RMCE), which was previously described (62–64). *TBX2* human reference and variants cDNA in pUASg-HA.attB constructs were injected into *y w φC31; VK00037* embryos (full genotype: *y[1] M{vas-int.Dm}ZH-2A w[*]; PBac{y[+]-attP-3B}VK00037*) (65) and transgenic flies were selected according to the mini-w^+ marker present on the transgenic construct. Lethality rescue experiments with BAC clones in *Drosophila* were performed by crossing *w[1118]/Y; Dp(1; 3)DC116/TM6c* males with *y w bifid[T2A-Gal4]/FM7c* virgin females (66,67). The males that have no *FM7c* balancer in the next generation were considered rescued flies. All flies were maintained at RT (~21°C). Crosses for rescue experiments were kept at either 18°C, 21°C or 25°C, all conditions showing the same results. All crosses for overexpression experiments were kept at 25°C.

Following strains of *Drosophila melanogaster* were used in this study.

Stocks obtained from Bloomington *Drosophila* Stock Center (BDSC) at Indiana University:

y w Mi{MIC}bi[MI08152]

y w T(1;2)bi[D2], bi[D2]/FM7c, sn[+]

y w[1118]; Dp(1;3)DC116, PBac{DC116}VK00033/TM6c, Sb (genomic rescue)

y w P{GAL4}bi[omb-Gal4], P{UAS-GFP.U}1 (bi[omb-Gal4])

y w; P{UAS-mCD8::GFP.L} (UAS-CD8::GFP)

y w[67c23]; P{dpp-Gal4.PS}6A/TM3, Ser (*dpp-Gal4*)

y w; P{w[+m]=GAL4-ey.H}4-8/CyO* (*ey-Gal4*)

y w; P{ry[+t7.2]=rh1-Gal4}1; ry[506] (*Rh1-Gal4*)

Stocks obtained from Dr. Gert Pflugfelder

y w hs-FLP; UAS-omb/CyO; MKRS/TM6b (UAS-bifid)

y w bi[D4]/FM7c

Stocks generated in-house for this study:

y w Mi{Trojan-Gal4.2}bi[MI08152-TG4.2]/FM7c (bi[T2A-Gal4])

y w; M[UAS-TBX2.ORF]VK00037/CyO (UAS-TBX2)

y w; M[UAS-TBX2-R20Q.ORF]VK00037/CyO (UAS-TBX2[R20Q])

y w; M[UAS-TBX2-R305H.ORF]VK00037/CyO (UAS-TBX2[R305H])

Light microscopy and imaging of *Drosophila*

Images of the *Drosophila* eyes were taken using a digital camera (MicroFire; Olympus) mounted on a stereomicroscope (MZ16; Leica) using ImagePro Plus 5.0 acquisition software (Media Cybernetics). The 'extend depth of field' function of the AxioVision software was used to obtain stack images by focus stacking.

ERG recording

ERG recordings were performed as previously described (42). Briefly, adult flies were glued to a glass slide, a recording electrode was placed on the surface of the eye while a reference probe was inserted in the thorax. The flies were exposed to a flash of white light for 1 s. Responses were recorded and analyzed with AXON^{TM}-pCLAMP8 software. Data were analyzed by two-tailed unpaired Student's *t*-test. A *P*-value of <0.05 was considered statistically significant.

Supplementary Material

Supplementary Material is available at *HMG* online.

Acknowledgements

We are grateful to the patients and their families who contributed to this study and allowed us to publish their information and pictures. We thank Drs. Kenneth L. Scott (*TBX2* cDNA), Antonio Baldini (luciferase assay reagents) and Gert Pflugfelder (Bifid antibody and *Drosophila* stocks) for providing valuable reagents used in this study. We thank Dr. Karen L. Schulze for critical reading and editing of this manuscript.

Conflict of Interest statement. Z.P., K.R. and C.M. are employed by Ambry Genetics. Exome sequencing is a commercially available test.

Funding

National Institutes of Health (NIH) (U01HG007672 to V.S., U54NS093793, R01GM067858, R24OD022005 to H.J.B.). Confocal microscopy at BCM is supported in part by NIH Grant U54HD083092 to the Intellectual and Developmental Disabilities Research Center (IDDRC) Neurovisualization Core. M.F.W. and S.Y. received support from the Simons Foundation (SFARI: 368479). H.J.B. is an investigator of the Howard Hughes Medical Institute.

References

1. Arnold, S.J., Hofmann, U.K., Bikoff, E.K. and Robertson, E.J. (2008) Pivotal roles for eomesodermin during axis formation, epithelium-to-mesenchyme transition and endoderm specification in the mouse. *Development*, **135**, 501–511.
2. Duboc, V. and Logan, M.P. (2011) Regulation of limb bud initiation and limb-type morphology. *Dev. Dyn.*, **240**, 1017–1027.
3. Greulich, F., Rudat, C. and Kispert, A. (2011) Mechanisms of T-box gene function in the developing heart. *Cardiovasc. Res.*, **91**, 212–222.
4. Kispert, A., Koschorz, B. and Herrmann, B.G. (1995) The T protein encoded by Brachyury is a tissue-specific transcription factor. *EMBO J.*, **14**, 4763–4772.
5. Ouimette, J.F., Jolin, M.L., L'Honore, A., Gifuni, A. and Drouin, J. (2010) Divergent transcriptional activities determine limb identity. *Nat. Commun.*, **1**, 1.
6. Lindsay, E.A., Vitelli, F., Su, H., Morishima, M., Huynh, T., Pramparo, T., Jurecic, V., Ogunrinu, G., Sutherland, H.F., Scambler, P.J. *et al.* (2001) Tbx1 haploinsufficieny in the DiGeorge syndrome region causes aortic arch defects in mice. *Nature*, **410**, 97–101.
7. Merscher, S., Funke, B., Epstein, J.A., Heyer, J., Puech, A., Lu, M.M., Xavier, R.J., Demay, M.B., Russell, R.G., Factor, S. *et al.* (2001) TBX1 is responsible for cardiovascular defects in velo-cardio-facial/DiGeorge syndrome. *Cell*, **104**, 619–629.
8. Bamshad, M., Lin, R.C., Law, D.J., Watkins, W.C., Krakowiak, P.A., Moore, M.E., Franceschini, P., Lala, R., Holmes, L.B., Gebuhr, T.C. *et al.* (1997) Mutations in human TBX3 alter limb, apocrine and genital development in ulnar-mammary syndrome. *Nat. Genet.*, **16**, 311–315.
9. Bongers, E.M., Duijf, P.H., van Beersum, S.E., Schoots, J., Van Kampen, A., Burckhardt, A., Hamel, B.C., Losan, F., Hoefsloot, L.H., Yntema, H.G. *et al.* (2004) Mutations in the human TBX4 gene cause small patella syndrome. *Am. J. Hum. Genet.*, **74**, 1239–1248.
10. Basson, C.T., Bachinsky, D.R., Lin, R.C., Levi, T., Elkins, J.A., Soults, J., Grayzel, D., Kroumpouzou, E., Traill, T.A., Leblanc-Straceski, J. *et al.* (1997) Mutations in human TBX5 cause limb and cardiac malformation in Holt-Oram syndrome. *Nat. Genet.*, **15**, 30–35.
11. Li, Q.Y., Newbury-Ecob, R.A., Terrett, J.A., Wilson, D.I., Curtis, A.R., Yi, C.H., Gebuhr, T., Bullen, P.J., Robson, S.C., Strachan, T. *et al.* (1997) Holt-Oram syndrome is caused by mutations in TBX5, a member of the Brachyury (T) gene family. *Nat. Genet.*, **15**, 21–29.
12. Harrelson, Z., Kelly, R.G., Goldin, S.N., Gibson-Brown, J.J., Bollag, R.J., Silver, L.M. and Papaioannou, V.E. (2004) Tbx2 is essential for patterning the atrioventricular canal and for morphogenesis of the outflow tract during heart development. *Development*, **131**, 5041–5052.
13. Manning, L., Ohyama, K., Saeger, B., Hatano, O., Wilson, S.A., Logan, M. and Placzek, M. (2006) Regional morphogenesis in

the hypothalamus: a BMP-Tbx2 pathway coordinates fate and proliferation through Shh downregulation. *Dev. Cell*, **11**, 873–885.
14. Behesti, H., Papaioannou, V.E. and Sowden, J.C. (2009) Loss of Tbx2 delays optic vesicle invagination leading to small optic cups. *Dev. Biol.*, **333**, 360–372.
15. Borke, J.L., Chen, J.R., Yu, J.C., Bollag, R.J., Orellana, M.F. and Isales, C.M. (2003) Negative transcriptional regulation of connexin 43 by Tbx2 in rat immature coronal sutures and ROS 17/2.8 cells in culture. *Cleft Palate Craniofac. J.*, **40**, 284–290.
16. Nissim, S., Allard, P., Bandyopadhyay, A., Harfe, B.D. and Tabin, C.J. (2007) Characterization of a novel ectodermal signaling center regulating Tbx2 and Shh in the vertebrate limb. *Dev. Biol.*, **304**, 9–21.
17. Radio, F.C., Bernardini, L., Loddo, S., Bottillo, I., Novelli, A., Mingarelli, R. and Dallapiccola, B. (2010) TBX2 gene duplication associated with complex heart defect and skeletal malformations. *Am. J. Med. Genet. A*, **152A**, 2061–2066.
18. Ballif, B.C., Theisen, A., Rosenfeld, J.A., Traylor, R.N., Gastier-Foster, J., Thrush, D.L., Astbury, C., Bartholomew, D., McBride, K.L., Pyatt, R.E. *et al.* (2010) Identification of a recurrent microdeletion at 17q23.1q23.2 flanked by segmental duplications associated with heart defects and limb abnormalities. *Am. J. Hum. Genet.*, **86**, 454–461.
19. Ramoni, R.B., Mulvihill, J.J., Adams, D.R., Allard, P., Ashley, E.A., Bernstein, J.A., Gahl, W.A., Hamid, R., Loscalzo, J., McCray, A.T. *et al.* (2017) The Undiagnosed Diseases Network: accelerating discovery about health and disease. *Am. J. Hum. Genet.*, **100**, 185–192.
20. Sobreira, N., Schiettecatte, F., Valle, D. and Hamosh, A. (2015) GeneMatcher: a matching tool for connecting investigators with an interest in the same gene. *Hum. Mutat.*, **36**, 928–930.
21. Wang, J., Al-Ouran, R., Hu, Y., Kim, S.Y., Wan, Y.W., Wangler, M.F., Yamamoto, S., Chao, H.T., Comjean, A., Mohr, S.E. *et al.* (2017) MARRVEL: integration of human and model organism genetic resources to facilitate functional annotation of the human genome. *Am. J. Hum. Genet.*, **100**, 843–853.
22. Ng, P.C. and Henikoff, S. (2001) Predicting deleterious amino acid substitutions. *Genome Res.*, **11**, 863–874.
23. Adzhubei, I., Jordan, D.M. and Sunyaev, S.R. (2013) Predicting functional effect of human missense mutations using PolyPhen-2. Curr. Protoc. Hum. Genet., Chapter 7, Unit7 20.
24. Schwarz, J.M., Cooper, D.N., Schuelke, M. and Seelow, D. (2014) MutationTaster2: mutation prediction for the deep-sequencing age. *Nat. Methods*, **11**, 361–362.
25. Kircher, M., Witten, D.M., Jain, P., O'Roak, B.J., Cooper, G.M. and Shendure, J. (2014) A general framework for estimating the relative pathogenicity of human genetic variants. *Nat. Genet.*, **46**, 310–315.
26. Lek, M., Karczewski, K.J., Minikel, E.V., Samocha, K.E., Banks, E., Fennell, T., O'Donnell-Luria, A.H., Ware, J.S., Hill, A.J., Cummings, B.B. *et al.* (2016) Analysis of protein-coding genetic variation in 60,706 humans. *Nature*, **536**, 285–291.
27. Quinodoz, M., Royer-Bertrand, B., Cisarova, K., Di Gioia, S.A., Superti-Furga, A. and Rivolta, C. (2017) DOMINO: using machine learning to predict genes associated with dominant disorders. *Am. J. Hum. Genet.*, **101**, 623–629.
28. Firth, H.V., Richards, S.M., Bevan, A.P., Clayton, S., Corpas, M., Rajan, D., Van Vooren, S., Moreau, Y., Pettett, R.M. and Carter, N.P. (2009) DECIPHER: database of chromosomal imbalance and phenotype in humans using ensembl resources. *Am. J. Hum. Genet.*, **84**, 524–533.
29. Carreira, S., Dexter, T.J., Yavuzer, U., Easty, D.J. and Goding, C.R. (1998) Brachyury-related transcription factor Tbx2 and repression of the melanocyte-specific TRP-1 promoter. *Mol. Cell. Biol.*, **18**, 5099–5108.
30. Sinha, S., Abraham, S., Gronostajski, R.M. and Campbell, C.E. (2000) Differential DNA binding and transcription modulation by three T-box proteins, T, TBX1 and TBX2. *Gene*, **258**, 15–29.
31. Kispert, A. and Herrmann, B.G. (1993) The Brachyury gene encodes a novel DNA binding protein. *EMBO J.*, **12**, 3211–3220.
32. Bellen, H.J. and Yamamoto, S. (2015) Morgan's legacy: fruit flies and the functional annotation of conserved genes. *Cell*, **163**, 12–14.
33. Yoon, W.H., Sandoval, H., Nagarkar-Jaiswal, S., Jaiswal, M., Yamamoto, S., Haelterman, N.A., Putluri, N., Putluri, V., Sreekumar, A., Tos, T. *et al.* (2017) Loss of nardilysin, a mitochondrial co-chaperone for alpha-ketoglutarate dehydrogenase, promotes mTORC1 activation and neurodegeneration. *Neuron*, **93**, 115–131.
34. Chao, H.T., Davids, M., Burke, E., Pappas, J.G., Rosenfeld, J.A., McCarty, A.J., Davis, T., Wolfe, L., Toro, C., Tifft, C. *et al.* (2017) A syndromic neurodevelopmental disorder caused by de novo variants in EBF3. *Am. J. Hum. Genet.*, **100**, 128–137.
35. Pflugfelder, G.O., Roth, H., Poeck, B., Kerscher, S., Schwarz, H., Jonschker, B. and Heisenberg, M. (1992) The lethal(1)optomotor-blind gene of Drosophila melanogaster is a major organizer of optic lobe development: isolation and characterization of the gene. *Proc. Natl. Acad. Sci. U. S. A.*, **89**, 1199–1203.
36. Grimm, S. and Pflugfelder, G.O. (1996) Control of the gene optomotor-blind in Drosophila wing development by decapentaplegic and wingless. *Science*, **271**, 1601–1604.
37. Teng, H., Davis, E., Abrahams, A., Mowla, S., Parker, M.I. and Prince, S. (2007) A role for Tbx2 in the regulation of the alpha2(1) collagen gene in human fibroblasts. *J. Cell. Biochem.*, **102**, 618–625.
38. Shen, J., Dahmann, C. and Pflugfelder, G.O. (2010) Spatial discontinuity of optomotor-blind expression in the Drosophila wing imaginal disc disrupts epithelial architecture and promotes cell sorting. *BMC Dev. Biol.*, **10**, 23.
39. Harel, T., Yoon, W.H., Garone, C., Gu, S., Coban-Akdemir, Z., Eldomery, M.K., Posey, J.E., Jhangiani, S.N., Rosenfeld, J.A., Cho, M.T. *et al.* (2016) Recurrent de novo and biallelic variation of ATAD3A, encoding a mitochondrial membrane protein, results in distinct neurological syndromes. *Am. J. Hum. Genet.*, **99**, 831–845.
40. Bonini, N.M., Bui, Q.T., Gray-Board, G.L. and Warrick, J.M. (1997) The Drosophila eyes absent gene directs ectopic eye formation in a pathway conserved between flies and vertebrates. *Development*, **124**, 4819–4826.
41. Xu, H., Lee, S.J., Suzuki, E., Dugan, K.D., Stoddard, A., Li, H.S., Chodosh, L.A. and Montell, C. (2004) A lysosomal tetraspanin associated with retinal degeneration identified via a genome-wide screen. *EMBO J.*, **23**, 811–822.
42. Luo, X., Rosenfeld, J.A., Yamamoto, S., Harel, T., Zuo, Z., Hall, M., Wierenga, K.J., Pastore, M.T., Bartholomew, D., Delgado, M.R. *et al.* (2017) Clinically severe CACNA1A alleles affect synaptic function and neurodegeneration differentially. *PLoS Genet*, **13**, e1006905.
43. Minke, B., Wu, C.F. and Pak, W.L.J. (1975) Isolation of light-induced response of the central retinula cells from the electroretinogram of Drosophila. *J. Comp. Physiol.*, **98**, 345.
44. Thi Thu, H.N., Haw Tien, S.F., Loh, S.L., Bok Yan, J.S. and Korzh, V. (2013) Tbx2a is required for specification of

endodermal pouches during development of the pharyngeal arches. *PLoS One*, **8**, e77171.
45. Alvarez-Delfin, K., Morris, A.C., Snelson, C.D., Gamse, J.T., Gupta, T., Marlow, F.L., Mullins, M.C., Burgess, H.A., Granato, M. and Fadool, J.M. (2009) Tbx2b is required for ultraviolet photoreceptor cell specification during zebrafish retinal development. *Proc. Natl. Acad. Sci. U. S. A.*, **106**, 2023–2028.
46. Wakker, V., Brons, J.F., Aanhaanen, W.T., van Roon, M.A., Moorman, A.F. and Christoffels, V.M. (2010) Generation of mice with a conditional null allele for Tbx2. *Genesis*, **48**, 195–199.
47. Mesbah, K., Rana, M.S., Francou, A., van Duijvenboden, K., Papaioannou, V.E., Moorman, A.F., Kelly, R.G. and Christoffels, V.M. (2012) Identification of a Tbx1/Tbx2/Tbx3 genetic pathway governing pharyngeal and arterial pole morphogenesis. *Hum. Mol. Genet.*, **21**, 1217–1229.
48. McDonald-McGinn, D.M., Sullivan, K.E., Marino, B., Philip, N., Swillen, A., Vorstman, J.A., Zackai, E.H., Emanuel, B.S., Vermeesch, J.R., Morrow, B.E. *et al.* (2015) 22q11.2 deletion syndrome. *Nat. Rev. Dis. Primers*, **1**, 15071.
49. Papaioannou, V.E. (2014) The T-box gene family: emerging roles in development, stem cells and cancer. *Development*, **141**, 3819–3833.
50. Shashi, V., Pena, L.D., Kim, K., Burton, B., Hempel, M., Schoch, K., Walkiewicz, M., McLaughlin, H.M., Cho, M., Stong, N. *et al.* (2016) De novo truncating variants in ASXL2 are associated with a unique and recognizable clinical phenotype. *Am. J. Hum. Genet.*, **99**, 991–999.
51. Ropers, H.H. and Wienker, T. (2015) Penetrance of pathogenic mutations in haploinsufficient genes for intellectual disability and related disorders. *Eur. J. Med. Genet.*, **58**, 715–718.
52. Bainbridge, M.N., Hu, H., Muzny, D.M., Musante, L., Lupski, J.R., Graham, B.H., Chen, W., Gripp, K.W., Jenny, K., Wienker, T.F. *et al.* (2013) De novo truncating mutations in ASXL3 are associated with a novel clinical phenotype with similarities to Bohring-Opitz syndrome. *Genome Med.*, **5**, 11.
53. Tarailo-Graovac, M., Zhu, J.Y.A., Matthews, A., van Karnebeek, C.D.M. and Wasserman, W.W. (2017) Assessment of the ExAC data set for the presence of individuals with pathogenic genotypes implicated in severe Mendelian pediatric disorders. *Genet. Med.*, **19**, 1300–1308.
54. Johnston, J.J., Lewis, K.L., Ng, D., Singh, L.N., Wynter, J., Brewer, C., Brooks, B.P., Brownell, I., Candotti, F., Gonsalves, S.G. *et al.* (2015) Individualized iterative phenotyping for genome-wide analysis of loss-of-function mutations. *Am. J. Hum. Genet.*, **96**, 913–925.
55. MacArthur, D.G., Manolio, T.A., Dimmock, D.P., Rehm, H.L., Shendure, J., Abecasis, G.R., Adams, D.R., Altman, R.B., Antonarakis, S.E., Ashley, E.A. *et al.* (2014) Guidelines for investigating causality of sequence variants in human disease. *Nature*, **508**, 469–476.
56. Bick, D., Fraser, P.C., Gutzeit, M.F., Harris, J.M., Hambuch, T.M., Helbling, D.C., Jacob, H.J., Kersten, J.N., Leuthner, S.R., May, T. *et al.* (2017) Successful application of whole genome sequencing in a medical genetics clinic. *J. Pediatr. Genet.*, **6**, 61–76.
57. Farwell, K.D., Shahmirzadi, L., El-Khechen, D., Powis, Z., Chao, E.C., Tippin Davis, B., Baxter, R.M., Zeng, W., Mroske, C., Parra, M.C. *et al.* (2015) Enhanced utility of family-centered diagnostic exome sequencing with inheritance model-based analysis: results from 500 unselected families with undiagnosed genetic conditions. *Genet. Med.*, **17**, 578–586.
58. Farwell Hagman, K.D., Shinde, D.N., Mroske, C., Smith, E., Radtke, K., Shahmirzadi, L., El-Khechen, D., Powis, Z., Chao, E.C., Alcaraz, W.A. *et al.* (2017) Candidate-gene criteria for clinical reporting: diagnostic exome sequencing identifies altered candidate genes among 8% of patients with undiagnosed diseases. *Genet. Med.*, **19**, 224–235.
59. Zweier, C., Sticht, H., Aydin-Yaylagul, I., Campbell, C.E. and Rauch, A. (2007) Human TBX1 missense mutations cause gain of function resulting in the same phenotype as 22q11.2 deletions. *Am. J. Hum. Genet.*, **80**, 510–517.
60. Fulcoli, F.G., Huynh, T., Scambler, P.J. and Baldini, A. (2009) Tbx1 regulates the BMP-Smad1 pathway in a transcription independent manner. *PLoS One*, **4**, e6049.
61. Lee, P.T., Lin, H.W., Chang, Y.H., Fu, T.F., Dubnau, J., Hirsh, J., Lee, T. and Chiang, A.S. (2011) Serotonin-mushroom body circuit modulating the formation of anesthesia-resistant memory in Drosophila. *Proc. Natl. Acad. Sci. U. S. A.*, **108**, 13794–13799.
62. Venken, K.J., Schulze, K.L., Haelterman, N.A., Pan, H., He, Y., Evans-Holm, M., Carlson, J.W., Levis, R.W., Spradling, A.C., Hoskins, R.A. *et al.* (2011) MiMIC: a highly versatile transposon insertion resource for engineering Drosophila melanogaster genes. *Nat. Methods*, **8**, 737–743.
63. Nagarkar-Jaiswal, S., Lee, P.T., Campbell, M.E., Chen, K., Anguiano-Zarate, S., Gutierrez, M.C., Busby, T., Lin, W.W., He, Y., Schulze, K.L. *et al.* (2015) A library of MiMICs allows tagging of genes and reversible, spatial and temporal knockdown of proteins in Drosophila. *Elife*, **4**,
64. Lee, P.T., Zirin, J., Kanca, O., Lin, W.W., Schulze, K.L., Li-Kroeger, D., Tao, R., Devereaux, C., Hu, Y., Chung, V. *et al.* (2018) A gene-specific T2A-GAL4 library for Drosophila. *Elife*, **7**, e35574.
65. Venken, K.J., He, Y., Hoskins, R.A. and Bellen, H.J. (2006) P[acman]: a BAC transgenic platform for targeted insertion of large DNA fragments in D. melanogaster. *Science*, **314**, 1747–1751.
66. Venken, K.J., Carlson, J.W., Schulze, K.L., Pan, H., He, Y., Spokony, R., Wan, K.H., Koriabine, M., de Jong, P.J., White, K.P. *et al.* (2009) Versatile P[acman] BAC libraries for transgenesis studies in Drosophila melanogaster. *Nat. Methods*, **6**, 431–434.
67. Venken, K.J., Popodi, E., Holtzman, S.L., Schulze, K.L., Park, S., Carlson, J.W., Hoskins, R.A., Bellen, H.J. and Kaufman, T.C. (2010) A molecularly defined duplication set for the X chromosome of Drosophila melanogaster. *Genetics*, **186**, 1111–1125.